JOURNAL OF MAGNETIC RESONANCE **133,** 313–323 (1998)
ARTICLE NO. MN981455

INEPT Experiments Involving Quadrupolar Nuclei in Solids

Hsien-Ming Kao and Clare P. Grey

Department of Chemistry, State University of New York at Stony Brook, Stony Brook, New York 11794-3400

Received October 13, 1997; revised March 9, 1998

Coherence transfer from quadrupolar ^{27}Al ($I = \frac{5}{2}$) nuclei to ^{31}P ($I = \frac{1}{2}$) via INEPT experiments is investigated. ^{27}Al → ^{31}P INEPT experiments on a $(CH_3)_3P$–$AlCl_3$ complex in zeolite NaX are performed, and the results demonstrate that the ^{31}P INEPT signals strongly depend on whether or not the ^{27}Al pulses are applied synchronously with the rotor period, and on the length of the ^{27}Al pulses. A density-matrix calculation involving the use of the spin operators for spin $\frac{3}{2}$ and $\frac{1}{2}$ nuclei has been performed to help understand the evolution behavior of the density matrix under the influence of the quadrupolar interaction, the dipolar and *J*-couplings, and the pulse lengths applied to the quadrupolar nuclei. The theoretical predictions obtained from these calculations are consistent with the INEPT experimental observations. © 1998 Academic Press

Key Words: ***J*-coupling; INEPT; $(CH_3)_3P$–$AlCl_3$; density matrix; quadrupolar nuclei.**

INTRODUCTION

Coherence transfer via the *J*-coupling is one method often used to study spin–spin interactions between nuclei in solution NMR. Efforts have also been made to apply these methods in the solid state: for example, homonuclear *J*-coupling NMR methods (COSY and INADEQUATE) have previously been used by Fyfe *et al.* to establish the ^{29}Si–O–^{29}Si connectivities in zeolites (*1*). Klinowski and coworkers reported that the 2D *J*-scaled ^{29}Si COSY experiment can improve the spectral resolution for a sample of highly siliceous mordenite (*2*). More recently, Fyfe *et al.* demonstrated that coherence transfer via heteronuclear *J*-coupling between spin $\frac{1}{2}$ and quadrupolar nuclei can be achieved in the solid state with INEPT and DEPT experiments (*3*). We have employed the INEPT experiment to probe the interaction between surfaces and surface-bound species, for the first time, and have determined a ^{31}P–^{27}Al *J*-coupling constant of 270 ± 10 Hz for trimethylphosphine (TMP) bound to a Lewis acid site in dehydroxylated HY with a ^{27}Al → ^{31}P INEPT experiment (*4*). In this work, we present the results of a systematic investigation of the ^{27}Al → ^{31}P INEPT experiment for a TMP–$AlCl_3$ complex in NaX. Density matrix calculations are performed to improve the understanding of the INEPT experiment involving noninteger spins in the solid state, under magic angle spinning (MAS) conditions. An $I = \frac{1}{2}$, $S = \frac{3}{2}$ spin system is chosen to simplify the calculations. Results from these calculations are then employed to help rationalize and explain the experimental observations.

EXPERIMENTAL

Zeolite NaX was dehydrated by slowly heating up an approximately 0.3 g sample to 400°C over a period of 16 h in a vacuum system. Subsequently, anhydrous $AlCl_3$ (Alfa) was physically mixed with the NaX sample in a glove box, under an inert N_2 atmosphere, and the resulting sample was heated at 80°C for a couple of hours. TMP (Alfa) was then introduced onto the resulting zeolite sample through the vacuum line and excess TMP was removed by degassing the sample at room temperature.

Solid-state NMR experiments were performed with a Chemagnetics CMX360 spectrometer equipped with a triple-tuned 7.5-mm probe which was tuned to the Larmor frequencies of the ^{1}H, ^{27}Al, and ^{31}P nuclei. ^{31}P chemical shifts are reported relative to 85% H_3PO_4. The standard INEPT sequence, with appropriate phase cycling, was employed for the ^{27}Al → ^{31}P INEPT experiments and is shown below (*5*):

$$\begin{array}{ll} ^{27}\mathrm{Al} & (\Theta)_y - \tau - (2\Theta)_y - \tau - (\Theta)_{\pm x} \\ ^{31}\mathrm{P} & \qquad\qquad (\pi)_y \quad - \tau - (\pi/2)_y - \mathrm{Acquire}. \end{array}$$

Here $(\Theta)_y$ is a pulse of length Θ/ω_1. Two sets of experiments were performed. In the first, all the pulses were applied synchronously with the rotor period (i.e., $\tau = (n/\nu_r)$, where ν_r is the spinning speed, and n is an integer). In the second, the pulses were applied asynchronously with the rotor period. INEPT spectra were acquired as a function of Θ and τ. An ^{27}Al RF field strength of 55 kHz, measured with aqueous aluminum sulfate, was used to excite the ^{27}Al spins. This corresponds to a $\pi/2$ pulse length for aluminum sulfate of 4.5 μs. ^{31}P $\pi/2$ pulse lengths of 6 μs and repetition times of 1 s were employed.

RESULTS

The ^{31}P MAS NMR spectrum of a TMP–$AlCl_3$ complex in NaX is shown in Fig. 1a. A sextet is observed at −43 ppm

1090-7807/98 $25.00

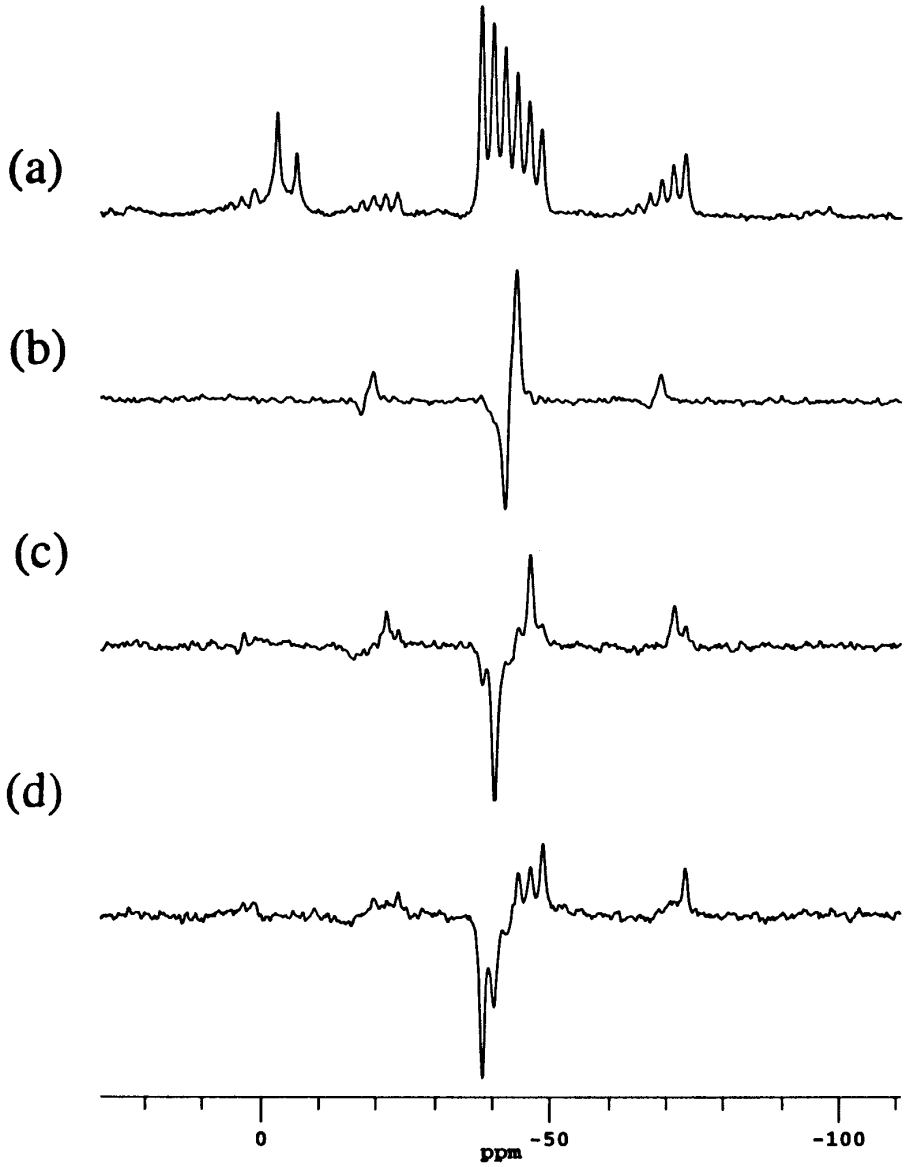

FIG. 1. The influence of the pulse lengths applied to the ^{27}Al spins on the ^{27}Al $\rightarrow$ ^{31}P INEPT spectra of a TMP–$AlCl_3$ complex in zeolite NaX. (a) ^{31}P one-pulse MAS spectrum. (b)–(d); ^{27}Al $\rightarrow$ ^{31}P INEPT spectra obtained with different ^{27}Al Θ and 2Θ pulses: (b) $\Theta = \pi/6$ (1.5 μs) and $2\Theta = \pi/3$ (3.0 μs), (c) $\Theta = \pi/3$ (3.0 μs) and $2\Theta = 2\pi/3$ (6.0 μs), and (d) $\Theta = \pi/2$ (4.5 μs) and $2\Theta = \pi$ (9.0 μs). ^{27}Al RF strength = 55 kHz; spinning speed = 3.6 kHz; the evolution time (τ) = 0.75 ms.

with a ^{31}P–^{27}Al *J*-coupling constant of ca. 300 Hz, which results from *J*-coupling to the six Zeeman levels of ^{27}Al. This is consistent with previous studies of the TMP–$AlCl_3$ complex in HY and NaHY (*6*). In addition, a much less intense doublet was also observed at around -2 ppm, with a ^{31}P–^{1}H *J*-coupling constant of ca. 550 Hz (*7*). This is due to the protonated TMP species ($TMPH^+$), formed from reaction of TMP with acidic protons, possibly associated with the $AlCl_3$. Figures 1b–1d show the ^{27}Al $\rightarrow$ ^{31}P INEPT spectra obtained under nonrotor synchronized conditions with various values for Θ and 2Θ. A maximum INEPT signal is achieved in principle, for a value for τ of $1/4J$ (0.833 ms), assuming $T_2 \gg 1/J$ and thus, the value of τ used to acquire these spectra (0.75 ms) was chosen because it was close to this optimal value but far from a multiple of the rotor period ($1/\nu_r = 0.277$ ms). Only the ^{27}Al $|+\frac{1}{2}\rangle$ and $|-\frac{1}{2}\rangle$ states coupled to ^{31}P give rise to INEPT signals when short pulses (i.e., $\Theta = \pi/6$ and $2\Theta = \pi/3$, or 1.5 and 3.0 μs, respectively) were applied to the ^{27}Al spins (Fig. 1b). No significant INEPT signals due to the coupling to ^{27}Al in the $|\pm\frac{3}{2}\rangle$ and $|\pm\frac{5}{2}\rangle$ states were observed. However, as the values for Θ and 2Θ were increased, peaks arising from coupling to $|\pm\frac{3}{2}\rangle$ and $|\pm\frac{5}{2}\rangle$ states were also observed: When $\Theta = \pi/3$ (and $2\Theta = 2\pi/3$), peaks corresponding to the $|\pm\frac{3}{2}\rangle$ states are the

most intense peaks in the INEPT sextet (Fig. 1c), and only small peaks are observed due to the $|\pm\frac{5}{2}\rangle$ states, while those from the central $|\pm\frac{1}{2}\rangle$ states are extremely small. When Θ is increased to $\pi/2$, peaks corresponding to the $|\pm\frac{5}{2}\rangle$ states are now the most intense (Fig. 1d). Note that the magnitude of the intensities of the ^{31}P spins coupled to the $|+\frac{5}{2}\rangle$ and $|-\frac{5}{2}\rangle$ states in the isotropic resonances are not equal, because some of the intensity is distributed in the sidebands.

Coherence transfer between all ^{27}Al six Zeeman states and ^{31}P was achieved when ^{27}Al $\pi/2$ and π pulses were applied synchronously with the rotor period (Fig. 2b). The relative intensities of the individual peaks within the ^{31}P INEPT sextet were not very sensitive to the pulse lengths applied to the ^{27}Al spins, as long as the ^{27}Al $\pi/2$ and π pulses are applied synchronously with the rotor period. However, small variations were observed. For example, the intensities of the ^{31}P resonances coupled to the $|+\frac{5}{2}\rangle$ and $|-\frac{5}{2}\rangle$ states are more intense when $\Theta = \pi/2$ pulses are used, and peaks corresponding to the $|\pm\frac{3}{2}\rangle$ states are maximized for $\Theta = \pi/3$. A significant reduction in the intensities of the ^{31}P INEPT signals was observed when ^{27}Al values for Θ greater than $\pi/2$ (4.5 μs) were employed.

FIG. 2. ^{27}Al $\rightarrow$ ^{31}P INEPT spectra of TMP–$AlCl_3$ complex in zeolite NaX obtained when ^{27}Al $\Theta = \pi/6$ and $2\Theta = \pi/3$ pulses (1.5 and 3.0 μs) were applied (a) asynchronously and (b) synchronously with the rotor period. Evolution times (τ) of 0.75 and 0.833 ms were used, respectively. Spinning speed = 3.6 kHz; ^{27}Al RF strength = 55 kHz. Spectra have been plotted on the same scale.

DENSITY-MATRIX CALCULATIONS FOR AN $I = \frac{1}{2}$, $S = \frac{3}{2}$ SPIN PAIR

Density-matrix calculations were performed for the INEPT experiment in order to rationalize some of the experimental observations. Calculations were carried out for the $I = \frac{1}{2}$, $S = \frac{3}{2}$ spin pair system to simplify the calculations considerably. Many of the conclusions obtained from the $I = \frac{1}{2}$, $S = \frac{3}{2}$ system can be readily applied to the spin-$\frac{5}{2}$ system, and the calculations and the experimental results will be compared in the Discussion section. The matrix representations of the $S = \frac{3}{2}$ spin operators S_x, S_y, and S_z are listed in Appendix 1. A set of $S = \frac{3}{2}$ spin operators listed in Appendix 2 was first introduced by Vega to investigate the MAS spin-locking of quadrupolar nuclei (*8*, *9*). These matrices are representations of the operators in the basis set of the spin wave functions $|\frac{3}{2}\rangle$, $|\frac{1}{2}\rangle$, $|-\frac{1}{2}\rangle$, and $|-\frac{3}{2}\rangle$. Among these spin operators, C_i and T_i ($i = x, y, z$) are associated with the central transition and triple-quantum coherence operators, respectively. R_x and R_y represent single-quantum coherence operators associated with the satellite transitions. Obviously, any operator T_i commutes with any operator C_j ($i, j = x, y, z$). The quadrupole operator, $[S_z^2 - S(S + 1)/3]$, can be rewritten as $\sqrt{8}Q_z$ and thus, the first-order quadrupole Hamiltonian H_Q is given by $\sqrt{2}Q'Q_z$ where Q', the quadrupole splitting, is given by $(\omega_Q/2)[3\cos^2\theta - 1 + \eta\sin^2\theta\cos 2\phi]$. θ and ϕ are the polar angles that define the orientation of the external magnetic field with respect to the electric field gradient principal axis system, η is the asymmetry parameter, and $\omega_Q = 3e^2qQ/[2S(2S-1)]$ is the quadrupole frequency. Useful commutation relations of these spin operators under the influence of the quadrupolar interaction (H_Q) and RF pulses (S_x, S_y, and S_z) are listed in Appendix 3.

If a pair of basis set operators O_a and O_b fulfills, with O_c, commutation relations of the form

$$i[O_a, O_c] = nO_b, \quad i[O_b, O_c] = -nO_a, \qquad [1]$$

then under the Hamiltonian $H = \omega_c O_c$, $\rho = O_a$ will evolve according to (*7*)

$$\exp(-i\omega_c O_c t)O_a\exp(i\omega_c O_c t) = O_a\cos(n\omega_c t) + O_b\sin(n\omega_c t). \qquad [2]$$

As seen from Appendix 3, the operators associated with the outer satellite transitions R_x, R_y, J_x, and J_y have commutation relations with H_Q following Eq. [1], and thus general expressions for the evolution of these operators can be readily derived from Eq. [2] and are listed in Table 1.

On the other hand, $[O_c, O_a] = O_b$ and $[O_c, O_b] = nO_a$, and $O_a \neq kO_b$, where n and k are constants, then the evolution of $\rho = O_a$ under the influence of the Hamiltonian $H = \omega_c O_c$ can be expressed as (*10*)

TABLE 1
The Evolution of R_x, R_y, J_x, and J_y under the Influence of H_Q

$$R_x \rightarrow R_x\cos Q't - J_x\sin Q't$$
$$J_x \rightarrow J_x\cos Q't + R_x\sin Q't$$
$$R_y \rightarrow R_y\cos Q't - J_y\sin Q't$$
$$J_y \rightarrow J_y\cos Q't + R_y\sin Q't$$

$$\exp(-i\omega_c O_c t)O_a\exp(i\omega_c O_c t) = O_a\cos(\sqrt{n}\omega_c t) - (i/\sqrt{n})O_b\sin(\sqrt{n}\omega_c t). \qquad [3]$$

The effect of the scalar J-coupling ($H_J = 2\pi J I_z S_z$) on a two-spin system (I and S) with an initial density matrix $\rho(0) = R_x$ can be considered in the following way. The commutation relations between the spin operators R_x and R_y and the operator I_zS_z are given by (see Appendix 3)

$$[I_zS_z, R_x] = iI_zR_y \qquad [4]$$

$$[I_zS_z, iI_zR_y] = -iI_z^2[R_y, S_z] = 1/4\ R_x, \qquad [5]$$

where we have rewritten Eq. [5] by making use of the fact that I_z^2 is equal to $\frac{1}{4}$ for a $I = \frac{1}{2}$ nucleus. The evolution of the density matrix $\rho(0) = R_x$ under the influence of the J-coupling can now be easily calculated from Eq. [3] and is given by

$$\exp(-iI_zS_z2\pi Jt)R_x\exp(iI_zS_z2\pi Jt) = R_x\cos\pi Jt + 2I_zR_y\sin\pi Jt. \qquad [6]$$

Analogous expressions for the evolution of other coherences under the influence of the J-coupling interaction are listed in Table 2.

Considering now the following INEPT pulse sequence applied to an isolated I ($I = \frac{1}{2}$) − S ($I = \frac{3}{2}$) pair (*11*):

S $\quad (\pi/2)_y - \tau - (\pi)_y - \tau - (\pi/2)_x$

I $\qquad\qquad\qquad\qquad (\pi)_y - \tau - (\pi/2)_y -$ Acquire.

At thermal equilibrium, the reduced density matrix for the S spins is S_z. The effect of the first $(\pi/2)_y$ pulse that is applied to the spin $S = \frac{3}{2}$ nuclei depends, however, on the size of the quadrupole coupling constant (QCC) of the $S = \frac{3}{2}$ nuclei. Two cases are considered here. First, for case (a): with small to moderate QCCs (i.e., the RF field strength applied to the S spins $\omega_1 \geq \omega_Q \neq 0$), the first $(\pi/2)_y$ pulse will excite both the central and satellite transitions. The density matrix after applying the first $(\pi/2)_y$ pulse is given by

$$\rho(0^+) = S_x = 2C_x + \sqrt{6}R_x, \qquad [7]$$

where C_x and R_x represent the terms in the density matrix that correspond to the central transition and satellite transitions, respectively (see Appendix 2). When the QCC is large (i.e., $\omega_1 \ll \omega_Q$) (case (b)), only the central transition is efficiently excited by the first pulse, for on-resonance irradiation, and thus the density matrix after a $(\pi/2)_y$ pulse is now given by

$$\rho(0^+) = C_x. \qquad [8]$$

The central transition coherence nutates at a frequency of $2\nu_1$ (for $\omega_1 \ll \omega_Q$) when an on-resonance RF field is applied, and the length of the $(\pi/2)_y$ pulse is now given by $\frac{1}{8\nu_1}$. The coefficients of terms involving C_x in the density matrices given in Eqs. [7] and [8] differ by a factor of two. Thus the intensities of the resonances in one-pulse spectra obtained from $S = \frac{3}{2}$ nuclei are dependent on the QCCs of different species, if a pulse of length $\frac{1}{2\nu_1}$ (or $1/\nu_1$) is applied. Bloch-decay spectra are not, therefore, always quantitative unless a short pulse is used (*12*).

Following the first pulse, the $S = \frac{3}{2}$ spins evolve under the influence of the quadrupolar interaction, and the dipolar and *J*-couplings,

$$H = \sqrt{2}Q'(t)Q_z + \omega_D(t)I_zS_z + 2\pi JI_zS_z, \qquad [9]$$

where $\sqrt{2}Q'(t)Q_z$, and $\omega_D(t)I_zS_z$ represent the secular part of the quadrupole Hamiltonian (H_Q), and the dipolar coupling Hamiltonian (H_D), respectively. The time dependence of Q' and the dipolar frequency (ω_D) must be included for the MAS experiment. Again, two cases are discerned. In the first, all the $\pi/2$ pulses are applied synchronously with the rotor period. In this case, the evolution of the spins under H_Q and H_D is averaged to zero over the whole evolution period. However, if the pulses are applied asynchronously, then we must consider evolution under all the terms given in Eq. [9]. The effect of chemical-shift evolution is ignored here, since the evolution of the *S* spins under the chemical shift Hamiltonian is refocused by the $(\pi)_y$ pulses, and thus no net evolution of the chemical shift occurs. The evolution of the density matrix $\rho(t)$ can be obtained by solving the Liouville–von Neumann equation separately since all the terms in the Hamiltonian commute with each other. For simplicity, any effects due to T_2 are assumed to be negligible. The reduced density matrix of the *S* spins during the first and second evolution periods (τ) of the INEPT experiment is derived below.

Case (a): Small to Moderate QCCs

The evolution of the central transition coherence C_x, under H_Q and H_D during the first evolution period, is shown schematically as

TABLE 2
The Evolution of C_x, C_y, R_x, R_y, J_x, and J_y under the Influence of *J*-coupling ($H_J = 2\pi JI_zS_z$)

$$\begin{aligned}
C_x &\rightarrow C_x\cos\pi Jt + 2I_zC_y\sin\pi Jt\\
C_y &\rightarrow C_y\cos\pi Jt - 2I_zC_x\sin\pi Jt\\
R_x &\rightarrow R_x\cos\pi Jt + 2I_zR_y\sin\pi Jt\\
R_y &\rightarrow R_y\cos\pi Jt - 2I_zR_x\sin\pi Jt\\
J_x &\rightarrow J_x\cos\pi Jt + 2I_zJ_y\sin\pi Jt\\
J_y &\rightarrow J_y\cos\pi Jt - 2I_zJ_x\sin\pi Jt
\end{aligned}$$

Note. To calculate analogous expressions for evolution under the influence of the dipolar coupling, $2\pi J$ should be replaced by $\omega_D/2$.

$$2C_x \xrightarrow{H_Q} 2C_x \xrightarrow{\bar{\omega}_D I_z S_z} 2[C_x\cos(\bar{\omega}_D/2)\tau + 2I_zC_y\sin(\bar{\omega}_D/2)\tau], \qquad [10]$$

where we have made use of the expressions given in Table 2. $\bar{\omega}_D(\alpha, \beta)$ represents the average dipolar frequency during the evolution period, for a particular initial orientation of the dipolar coupling tensor with respect to the rotor axis (defined by α and β). When the $\pi/2$ and π pulses are applied to the *S* spins synchronously with the rotor period, $\bar{\omega}_D$ is zero for all values of α and β and thus the last term in Eq. [10], i.e., $2[C_x\cos(\bar{\omega}_D/2)\tau + 2I_zC_y\sin(\bar{\omega}_D/2)\tau]$ is reduced to $2C_x$. Further evolution of the density matrix $2C_x$ under the influence of the *J*-coupling is given by

$$2C_x \xrightarrow{2\pi JI_zS_z} 2(C_x\cos\pi J\tau + 2I_zC_y\sin\pi J\tau). \qquad [11]$$

Unlike C_x, R_x does not commute with H_Q (see Appendix 3) and R_x evolves as

$$\sqrt{6}R_x \xrightarrow{H_Q} \sqrt{6}(R_x\cos\bar{Q}'\tau - J_x\sin\bar{Q}'\tau), \qquad [12]$$

where $\bar{Q}'(\theta, \phi)$ represents the average quadrupole splitting over the evolution period for a particular orientation of the quadrupolar tensor with respect to the external magnetic field.

Rotor synchronized conditions. Assuming that the $\pi/2$ and π pulses are applied to the *S* spins synchronously with the rotor period, the quadrupole splitting averaged over an integral number of whole rotor period is also zero, and thus the term $\sqrt{6}(R_x\cos\bar{Q}'\tau - J_x\sin\bar{Q}'\tau)$ in Eq. [12] can be reduced to $\sqrt{6}R_x$. Further evolution of R_x under the influence of the dipolar and *J*-couplings is similar to that of C_x and can be schematically shown as

$$\sqrt{6}R_x \xrightarrow{\bar{\omega}_D I_z S_z} \sqrt{6}R_x \xrightarrow{2\pi J I_z S_z} \sqrt{6}(R_x \cos \pi J\tau + 2I_z R_y \sin \pi J\tau). \quad [13]$$

The $(\pi)_y$ pulses applied simultaneously to the I and S spins serve only to refocus the chemical shifts, since a $(\pi)_y$ pulse applied to the S spins leaves C_y and R_y unaltered and changes the sign of C_x and R_x. The evolution of the density matrix during the second evolution period can be treated in the same way as that during the first evolution period, and the expression for the density matrix after the second evolution period is given by

$$\rho(2\tau) = -2C_x \cos 2\pi J\tau - \sqrt{6}R_x \cos 2\pi J\tau - 4I_z C_y \sin 2\pi J\tau - 2\sqrt{6}I_z R_y \sin 2\pi J\tau. \quad [14]$$

Only the terms in Eq. [14] containing I_z will result in observable signals, following the final $\pi/2$ pulses, and thus only terms involving $I_z C_y$ and $I_z R_y$ need be considered further.

The effect of an RF pulse S_x with flip angle $\omega_1 t$, where ω_1 represents the RF field applied to the S spins and t is the pulse length, on the C_y and R_y terms can be determined in the following way. From Appendix 3, we can obtain the following commutation relations:

$$\begin{aligned}
i[C_y, S_x] &= 2C_z - \sqrt{3/2}L_y,\\
i[C_z, S_x] &= -2C_y + \sqrt{3/2}R_y,\\
i[L_y, S_x] &= -R_y + \sqrt{3/2}(C_y - T_y),\\
i[R_y, S_x] &= L_y - \sqrt{3/2}(C_z - T_z),\\
i[T_y, S_x] &= \sqrt{3/2}L_y,\\
i[T_z, S_x] &= -\sqrt{3/2}R_y.
\end{aligned}$$

A general expression for the spin operator C_y, under the influence of S_x (i.e., $H = \omega_1 S_x$), can then be written in terms of a linear combinations of six operators

$$C_y \xrightarrow{S_x} a(t)C_y + b(t)C_z + c(t)L_y + d(t)R_y + e(t)T_y + f(t)T_z \quad [15]$$

with real, time-dependent coefficients. These coefficients obey a set of differential equations that can be derived by substituting this expression into the Liouville–von Neumann equation, yielding

$$\begin{bmatrix} a' \\ b' \\ c' \\ d' \\ e' \\ f' \end{bmatrix} = \begin{bmatrix} 0 & -2 & \sqrt{3/2} & 0 & 0 & 0 \\ 2 & 0 & 0 & -\sqrt{3/2} & 0 & 0 \\ -\sqrt{3/2} & 0 & 0 & 1 & \sqrt{3/2} & 0 \\ 0 & \sqrt{3/2} & -1 & 0 & 0 & -\sqrt{3/2} \\ 0 & 0 & -\sqrt{3/2} & 0 & 0 & 0 \\ 0 & 0 & 0 & \sqrt{3/2} & 0 & 0 \end{bmatrix} \times \begin{bmatrix} a \\ b \\ c \\ d \\ e \\ f \end{bmatrix}, \quad [16]$$

where a', for example, represents the first derivative of the coefficient a with respect to time t. The above equation can be solved to give expressions for each of coefficients at time t, by substituting in their initial values at time $t = 0$, i.e., $a = 1$, and all other terms are zero. The effect of an S_x pulse on R_y can be calculated in a similar way. The final expressions for spin operators C_y and R_y under the influence of an S_x pulse as a function of pulse length t are summarized in Table 3. Thus C_y and R_y are converted to C_z, L_y, and T_z after the application of a $(\pi/2)_x$ pulse,

$$C_y \rightarrow -1/4\ C_z + \sqrt{3/8}L_y + 3/4\ T_z \quad [17]$$

$$R_y \rightarrow \sqrt{3/8}C_z - 1/2 L_y + \sqrt{3/8}\ T_z, \quad [18]$$

where L_y represents a double quantum antiphase term in the density matrix. However, summing together Eqs. [17] and [18] with the appropriate scaling factors for C_y and R_y of 2 and $\sqrt{6}$, respectively (from Eq. [7]), results in the cancellation of the L_y terms. Thus the effect of a $(\pi/2)_x$ pulse applied to the S spins on the terms in Eq. [14] that contain I_z is

$$-4I_z C_y \sin 2\pi J\tau - 2\sqrt{6}I_z R_y \sin 2\pi J\tau \xrightarrow{(\pi/2)_x} -2(C_z + 3T_z)I_z \sin(2\pi J\tau). \quad [19]$$

A $(\pi/2)_y$ pulse applied to the I spins converts I_z to I_x, and observable INEPT signals result from terms in the density matrix that are proportional to $(C_z + 3T_z)I_x \sin 2\pi J\tau$. The $C_z I_x$ and $3T_z I_x$ terms give rise to INEPT signals from I spins coupled to the central and outer Zeeman levels of the S spins, respec-

TABLE 3
The Effect of an RF Pulse S_x with Pulse Length t on Terms in the Density Matrix C_y and R_y

$$\rho\text{: } C_y \text{ (or } R_y) \xrightarrow{S_x} a(t)C_y + b(t)C_z + c(t)L_y + d(t)R_y + e(t)T_y + f(t)T_z$$

(i)	C_y	R_y
$a(t)$	$7/16 \cos \omega_1 t + 9/16 \cos 3\omega_1 t$	$3/4\sqrt{3/8} \cos \omega_1 t - 3/4\sqrt{3/8} \cos 3\omega_1 t$
$b(t)$	$5/16 \sin \omega_1 t + 9/16 \sin 3\omega_1 t$	$1/4\sqrt{3/8} \sin \omega_1 t - 3/4\sqrt{3/8} \sin 3\omega_1 t$
$c(t)$	$1/4\sqrt{3/8} \sin \omega_1 t - 3/4\sqrt{3/8} \sin 3\omega_1 t$	$-1/8 \sin \omega_1 t + 3/8 \sin 3\omega_1 t$
$d(t)$	$3/4\sqrt{3/8} \cos \omega_1 t - 3/4\sqrt{3/8} \cos 3\omega_1 t$	$5/8 \cos \omega_1 t + 3/8 \cos 3\omega_1 t$
$e(t)$	$3/16 \cos \omega_1 t - 3/16 \cos 3\omega_1 t$	$-1/4\sqrt{3/8} \cos \omega_1 t + 1/4\sqrt{3/8} \cos 3\omega_1 t$
$f(t)$	$9/16 \sin \omega_1 t - 3/16 \sin 3\omega_1 t$	$5/4\sqrt{3/8} \sin \omega_1 t + 1/4\sqrt{3/8} \sin 3\omega_1 t$
(ii)	$\omega_1 t = \pi/2$	$\omega_1 t = \pi$
	$C_y \rightarrow -1/4C_z + \sqrt{3/8}\, L_y + 3/4T_z$	$-C_y$
	$R_y \rightarrow \sqrt{3/8}C_z - 1/2L_y + \sqrt{3/8}T_z$	$-R_y$

Note. Expressions for the coefficients $a(t) - f(t)$ defined above (and in Eq. [15]) are given in (i). Explicit values for the coefficients, calculated for $\omega_1 t = \pi/2$ and π, are listed in (ii).

tively. The $\sin 2\pi J\tau$ term results in the sinusoidal evolution of the INEPT signal that is expected for a *J*-coupling mechanism.

Non-rotor-synchronized conditions. The average quadrupole splitting and dipolar frequency are no longer zero at the end of the evolution period if the $\pi/2$ and π pulses are not applied synchronously with the rotor period. Under such conditions, the effect of the quadrupolar interaction on the evolution of C_x can be ignored to first order since the spin operator C_x commutes with the secular terms in the quadrupole Hamiltonian $H_Q = \sqrt{2}Q'(t)Q_z$ (Appendix 3). In contrast, R_x evolves as $(R_x \cos \bar{Q}'\tau - J_x \sin \bar{Q}'\tau)$ under the influence of the much larger quadrupolar interaction (Table 1), where J_x represents an antiphase term in the density matrix associated with the satellite transitions. Since $Q'(t)$ depends on the orientation of the quadrupolar tensor with respect to the external magnetic field and varies throughout the powder (and during the rotor cycle), dephasing will occur. Terms involving R_y will also dephase since R_y evolves in the $R_x - J_x$ plane at a frequency $Q'(t)$ under the influence of H_Q. Since $Q' \gg J$ (and ω_D), and long evolution periods of the order of $1/2J$ are used in order to transfer magnetization effectively, significant dephasing will occur during this time. This dephasing will not be refocused by the $(\pi)_y$ pulse under non-rotor-synchronized conditions, allowing us to ignore the terms involving R_x and R_y. In other words, the contribution of R_x to the intensity of INEPT signals can be disregarded due to the very rapid dephasing of the outer satellite transition coherences under the influence of the quadrupole Hamiltonian.

The intensity of INEPT signals following the final $\pi/2$ pulses, resulting from the central and satellite transitions, depends on the coefficients of C_z and T_z, i.e., $b(t)$ and $f(t)$, respectively, from Eq. [15]. The dependence of $b(t)$ and $f(t)$ on the pulse length t is listed in Table 3 and is plotted in Fig. 3 for the evolution of C_y (central transition). At short pulse lengths, $b(t)$ grows very quickly, reaching a maximum at $\omega_1 t \approx \pi/6$, and C_y is then converted into a combination of C_z, L_y, and T_z. In contrast, $f(t)$ increases in size more slowly, reaching a maximum at $\omega_1 t = \pi/2$. Thus C_y is predominantly transferred to C_z and the production of T_z is minimal if short pulse lengths are used: for example, $f(t)$ is close to 0.1 at $\omega_1 t \approx \pi/6$. For short pulses, we therefore expect to only observe peaks in the INEPT spectrum resulting from the *I* spins coupled to the central two Zeeman levels of the *S* spins, and the INEPT signal is given by $-(\frac{5}{8} \sin \omega_1 t + \frac{9}{8} \sin 3\omega_1 t)C_z I_z \sin(2\pi J\tau)$, ignoring smaller terms involving T_z. Magnetization is transferred to the outer levels of the *S* spins when longer pulse lengths are applied, and peaks from these coupled spins should be observed in the INEPT spectrum under these conditions.

Case (b): Large QCCs

In this case, only the central transition is excited by the initial on-resonance pulse applied to the *S* spins, and the density matrix following the first pulse is C_x (see Eq. [8]). However, the *S* spins associated with the central transition nutate at twice the frequency (i.e., $2\omega_1$), under the influence of the RF pulse, as that in case (a). Thus an optimum conversion to C_x is effected by applying a $\pi/4$ pulse, where $\pi/2$ is the optimum pulse length determined for a sample with a small-to-zero QCC. (A $\pi/2$ pulse should then be used as the second pulse to focus evolution due to chemical shift offsets.) C_x evolves in the same way during the evolution period as described in case (a) to produce terms involving $I_z C_y$ (Eqs. [10] and [11]). The $I_z C_y$ terms are converted to $I_x C_z$ terms following the last two pulses on the *I* and *S* spins. An antiphase doublet will be observed in the INEPT spectrum, from *I* spins coupled

to the $|\pm\frac{1}{2}\rangle$ S states. If the pulses are applied asynchronously with the rotor period, a decrease in the intensity of the INEPT signal is expected, caused by interference arising from evolution under the dipolar coupling Hamiltonian, H_D. In addition, the second-order quadrupolar interaction may now become more important. Evolution under this interaction is refocused with the second pulse ($\pi/2$). Since this is a time-dependent interaction, however, the effectiveness of the refocusing will decrease if the pulses are applied asynchronously. Thus for large QCCs it will be especially important to apply pulses synchronously with the rotor period.

DISCUSSION

The adsorption of TMP on a mixture of HY zeolite and aluminum chloride results in two TMP–$AlCl_3$ complexes with different stoichiometries (TMP–$AlCl_3$ and $(TMP)_2$–$AlCl_3$) and aluminum coordination numbers of 4 and 5, respectively. These complexes have been extensively studied by Lunsford *et al.* (*7*), who reported ^{27}Al QCCs for the 4- and 5-coordinated TMP–$AlCl_3$ complexes of 0.373 and 4.70 MHz, respectively. The ^{27}Al RF strength (55 kHz) used in this work is almost equal to the quadrupole frequency of the former species (56 kHz), which is the complex present in our samples. Thus the intensities of the $^{27}\text{Al} \rightarrow {}^{31}\text{P}$ INEPT peaks are expected to show similar behavior to that predicted for case (a) ($\omega_1 \geq \omega_Q$) of the density-matrix calculation section. Some differences are expected, clearly, since the experimental data are for $S = \frac{5}{2}$ nuclei. As predicted, peaks due to coupling to all the Zeeman levels are observed in the rotor-synchronized experiment (Fig. 2b). Under these conditions, any evolution due to the first-order quadrupolar interaction and the dipolar coupling following the first pulse is eliminated and only evolution due to the J-coupling is observed. Under non-rotor-synchronized conditions, only peaks resulting from coupling to the ^{27}Al central states are observed for short ^{27}Al pulses (Θ and 2Θ) (Fig. 1b). This is consistent with the prediction that the evolution due to the quadrupolar interaction results in the dephasing of terms in the density matrix associated with the satellite transitions (i.e., R_x and R_y when $S = \frac{3}{2}$). This dephasing is not effectively refocused by the 2Θ pulse, and at the end of the evolution periods only terms involving C_x and C_yI_z remain.

Short Θ pulses result in the conversion of C_y to C_z and INEPT signals are only observed from coupling to the $|\pm\frac{1}{2}\rangle$ states, under non-rotor-synchronized conditions. When longer Θ pulses are applied to the quadrupolar nuclei, the percentage of magnetization associated with the outer Zeeman levels increases rapidly compared to that of the central levels (Fig. 3). The coefficients for terms in the density matrix ($a(t) - f(t)$, defined by Eq. [15]) following a pulse were evaluated for a $S = \frac{3}{2}$ nucleus. They are all functions of two separate terms that oscillate with frequencies of ω_1 and $3\omega_1$ (Table 3). Maximum conversion to C_z (i.e., $b(t)$) was calculated to occur at $\Theta \approx \pi/6$. The coefficient for T_z, $f(t)$, increases in magnitude for larger values of Θ, reaching a maximum at $\pi/2$. In addition, by $\Theta = \pi/2$, $b(t)$ has inverted in sign and is also opposite in sign to $f(t)$. (Notice, however, that even though the coefficients depend on terms that oscillate at three times the RF field strength, the nutation frequency of, for example, the off-diagonal term C_y is still ω_1, which is expected for $\omega_Q < \omega_1$, since $a(0) = a(\omega_1 t = 2\pi) = -a(\pi)$.) Similar behavior may be expected for a spin $\frac{5}{2}$ nucleus. Now, however, the coefficients in the density matrix that describe the effect of a pulse of length Θ on C_y are functions of three terms that oscillate with frequencies of ω_1, $3\omega_1$, and $5\omega_1$. The experiments follow the theoretical predictions, qualitatively, and the successive population of the $|\pm\frac{1}{2}\rangle$ levels, followed by the $|\pm\frac{3}{2}\rangle$ levels, and finally the $|\pm\frac{5}{2}\rangle$ ^{27}Al Zeeman levels, as the length of the final pulse applied to the ^{27}Al spins is increased, is consistent with expectations. Unlike predictions for $S = \frac{3}{2}$ coupled spins (Fig. 3), the phase of the signals from the ^{31}P spins connected to the $|\pm\frac{1}{2}\rangle$ states remains the same as those for $|\pm\frac{3}{2}\rangle$ and $|\pm\frac{5}{2}\rangle$ connected states; however, a minimum in intensity is observed for $\Theta = \pi/3$. This is consistent with the more rapid transfer of magnetization from the $|\pm\frac{1}{2}\rangle$ to $|\pm\frac{3}{2}\rangle$ states (and then to $|\pm\frac{5}{2}\rangle$) that is expected for $S = \frac{5}{2}$ nuclei (where the terms in the density matrix oscillate with three frequencies ω_1, $3\omega_1$, and $5\omega_1$).

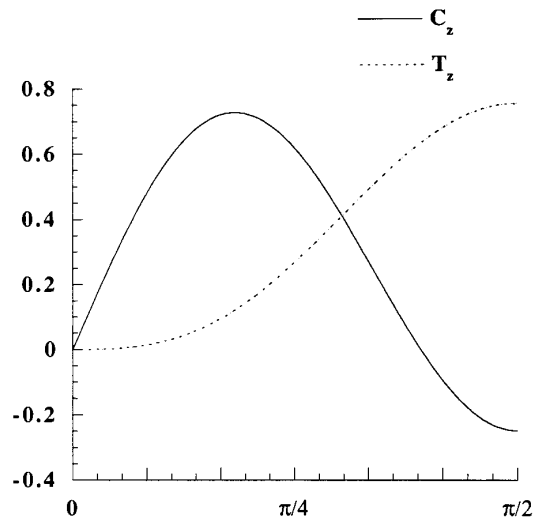

FIG. 3. The effect of a pulse of phase x represented by the operator S_x on the terms in the density matrix defined in Eq. [15], for an initial density matrix ($t = 0$): $\rho = C_x$. The values of the coefficients of C_z (solid line) and T_z (dashed line) are plotted as a function of the length of the pulse $\omega_1 t$ (in the range $\omega_1 t =$ 0 to $\pi/2$).

The intensities of the central and satellite transitions in one-pulse and echo spectra of noninteger spin quadrupolar nuclei have been studied in detail by P. Man (*13, 14*). The signal intensities were found to depend strongly on the pulse lengths applied to the quadrupolar nuclei and the ratio of the quadrupole frequency to the RF field strength. For simplicity, we have only explored the small QCC and large QCC regimes, and have not explored the effect of different pulse lengths on

the initial density matrix. In practice, the initial density matrix is more complicated than derived here, and the final INEPT signal intensities will depend, in principle, on the initial ratios of the coefficients of C_x and R_x following the application of the first pulse to the S spins. Our experimental data were acquired for the condition $\omega_Q \approx \omega_1$. Under these conditions, we are close to the intermediate regime for quadrupolar nuclei (intermediate between case (a) and (b)). In this regime, the nutation frequencies of the off-diagonal terms of the density matrix (e.g., C_x, R_x), under the influence of a pulse, are intermediate between ω_1 and $3\omega_1$ for $S = \frac{5}{2}$ (and ω_1 and $2\omega_1$ for $S = \frac{3}{2}$), and become a function of the orientation of the quadrupolar tensor to the external magnetic field. All parts of the powder pattern will not be excited evenly in our system, particularly for the $|\pm\frac{5}{2}\rangle - |\pm\frac{3}{2}\rangle$ outer satellite transitions. This is likely to be the major cause of the deviations in the INEPT spectra of the intensities (and phases) of the individual peaks of sextet (in the non-rotor-synchronized experiment) from those predicted from our model. The small variations in relative intensities of the six peaks, seen as a function of pulse length in the synchronized experiment, may also result from this. As demonstrated here, however, a simple density-matrix calculation which neglects the effect of the intermediate regime provides a satisfactory explanation for many of the INEPT experimental observations.

Our experimental observations, however, are not consistent with the results of INEPT experiments on a Ph_3P–$AlCl_3$ complex reported by Fyfe *et al.* (*3*). They observed ^{31}P INEPT signals resulting only from the central levels of the ^{27}Al spins, probably due to the relatively weak ^{27}Al RF strength (16 kHz) used in their experiments. Under these conditions, $\omega_Q > \omega_1$, and the experimental observations are expected to be close to the predictions for case (b). In addition, Fyfe *et al.* did not observe any additional peaks in the INEPT spectrum acquired under rotor synchronized experiments, which is again expected for case (b). This result is consistent with our earlier INEPT study of the complex formed when TMP binds to the Lewis acid site in the zeolite HY (*4*). We measured a QCC of close to 11 MHz for this complex (*4*), and thus $\omega_Q \gg \omega_1$ (case (b)). Again, only the central two peaks of the sextet were observed, consistent with predictions. Significant reductions in intensity were observed under non-rotor-synchronized conditions in the case of large QCC (*4*), due to dephasing caused by the dipolar coupling and the second-order quadrupolar interaction, which also varies throughout the rotor period. This observation is in contrast to the results of Fyfe *et al.* (*3*), who observed no attenuation of the INEPT signal in the non-rotor-synchronized experiment, even though $\omega_D \approx 2\pi J$. Thus, it is likely that the intensity reduction observed for the large QCC Lewis acid complex results in part from effects due to the second-order quadrupolar interaction. We have performed ^{1}H $\rightarrow$ ^{31}P INEPT experiments on the $TMPH^+$ complex formed in zeolite HY on TMP adsorption (*15*). This is the same species seen at ≈ -2 ppm in Fig. 1a. The ^{31}P–^{1}H J- and dipolar-coupled spin pair in this complex has a J-coupling constant of approximately 550 Hz (*7*) and a dipolar coupling constant of 34 kHz (*16*), and thus the dipolar coupling is the dominant interaction. In this case, although ^{31}P INEPT signals were observed under both synchronous and asynchronous conditions, a significant reduction of intensity was observed when the pulses were applied asynchronously with the rotor period. Thus a large intensity reduction, under non-rotor synchronized-conditions, is also to be expected for $\omega_D \gg 2\pi J$.

Finally, the INEPT signals under rotor-synchronized conditions from the $|\pm\frac{1}{2}\rangle$ states were observed to be less intense than those obtained under non-rotor-synchronized conditions (Figs. 2a and 2b). For $S = \frac{3}{2}$ nuclei, terms involving both I_zC_y and I_zR_y will contribute to the INEPT signals under rotor-synchronized conditions, following the final RF pulses on the I and S spins; however, only I_zC_y will contribute under non-rotor-synchronized conditions. The size of these terms can be evaluated from expressions listed in Table 3, and the intensity of the inner two peaks in the INEPT spectra is proportional to the size of the coefficient $b(t)$ (defined in Eq. [15]) following an RF pulse. For rotor-synchronized conditions, the contribution from R_y actually results in a reduction in the intensity of the central peaks of the INEPT spectrum for short pulses. Thus when $\Theta = \pi/6$ and $2\Theta = \pi/3$ pulses are applied, for example (conditions used in Fig. 2), the intensities of the INEPT signals resulting from the central states are calculated to be 0.5 and 1.44 for rotor- and non-rotor-synchronized conditions, respectively, where the coefficients ($b(t)$, Table 3), resulting from conversion of C_y and R_y (to C_z), have been scaled by factors of 2 and $\sqrt{6}$, respectively. A similar effect is expected for $S = \frac{5}{2}$ nuclei, and this prediction is in qualitative agreement with the experimental observations shown in Fig. 2.

CONCLUSIONS

Magnetization transfer via the J-coupling mechanism from all the six Zeeman levels of ^{27}Al was achieved for a TMP–$AlCl_3$ complex in NaX, in an ^{27}Al $\rightarrow$ ^{31}P INEPT experiment, by applying the ^{27}Al pulses synchronously with the rotor period. Under non-rotor-synchronized conditions, only ^{31}P spins coupled to the central states of ^{27}Al were observed in the INEPT spectrum when short pulses were applied to the ^{27}Al spins. However, the outer levels ($|\pm\frac{3}{2}\rangle$ and $|\pm\frac{5}{2}\rangle$) gave rise to the most intense ^{31}P INEPT signals when longer ^{27}Al pulses were employed. Simple density-matrix calculations involving the use of $S = \frac{3}{2}$ spin operators gave satisfactory explanations for many of the INEPT experimental observations.

A reduction in the intensities of the ^{31}P INEPT signals was observed when the pulses are not synchronized with the rotor period. Thus, for INEPT experiments involving quadrupolar nuclei in solids, where the evolution of the coherences associated with the outer satellite transitions, under the quadrupolar interaction, will be significant, and evolution under the dipolar coupling and second-order quadrupolar interaction (for a large QCC) may also be large, rotor synchronization of the pulses will be important to obtain optimal magnetization transfer.

APPENDIX 1

The Matrix Representations of the $S = 3/2$ Spin Operators S_x, S_y, and S_z

$$S_x = \frac{1}{2}\begin{bmatrix} 0 & \sqrt{3} & 0 & 0 \\ \sqrt{3} & 0 & 2 & 0 \\ 0 & 2 & 0 & \sqrt{3} \\ 0 & 0 & \sqrt{3} & 0 \end{bmatrix}; \quad S_y = \frac{1}{2}\begin{bmatrix} 0 & -i\sqrt{3} & 0 & 0 \\ i\sqrt{3} & 0 & -2i & 0 \\ 0 & 2i & 0 & -i\sqrt{3} \\ 0 & 0 & i\sqrt{3} & 0 \end{bmatrix}; \quad S_z = \frac{1}{2}\begin{bmatrix} 3 & 0 & 0 & 0 \\ 0 & 1 & 0 & 0 \\ 0 & 0 & -1 & 0 \\ 0 & 0 & 0 & -3 \end{bmatrix}$$

APPENDIX 2

Representations of the $S = 3/2$ Spin Operators in the Basis Set of the Spin Wave Functions $|\frac{3}{2}\rangle$, $|\frac{1}{2}\rangle$, $|-\frac{1}{2}\rangle$, and $|-\frac{3}{2}\rangle$ (after Refs. (*8*) and (*9*))

$$C_x = \frac{1}{2}\begin{bmatrix} 0 & 0 & 0 & 0 \\ 0 & 0 & 1 & 0 \\ 0 & 1 & 0 & 0 \\ 0 & 0 & 0 & 0 \end{bmatrix}; \quad C_y = \frac{1}{2}\begin{bmatrix} 0 & 0 & 0 & 0 \\ 0 & 0 & -i & 0 \\ 0 & i & 0 & 0 \\ 0 & 0 & 0 & 0 \end{bmatrix}; \quad C_z = \frac{1}{2}\begin{bmatrix} 0 & 0 & 0 & 0 \\ 0 & 1 & 0 & 0 \\ 0 & 0 & -1 & 0 \\ 0 & 0 & 0 & 0 \end{bmatrix}$$

$$T_x = \frac{1}{2}\begin{bmatrix} 0 & 0 & 0 & 1 \\ 0 & 0 & 0 & 0 \\ 0 & 0 & 0 & 0 \\ 1 & 0 & 0 & 0 \end{bmatrix}; \quad T_y = \frac{1}{2}\begin{bmatrix} 0 & 0 & 0 & -i \\ 0 & 0 & 0 & 0 \\ 0 & 0 & 0 & 0 \\ i & 0 & 0 & 0 \end{bmatrix}; \quad T_z = \frac{1}{2}\begin{bmatrix} 1 & 0 & 0 & 0 \\ 0 & 0 & 0 & 0 \\ 0 & 0 & 0 & 0 \\ 0 & 0 & 0 & -1 \end{bmatrix}$$

$$R_x = \frac{1}{\sqrt{8}}\begin{bmatrix} 0 & 1 & 0 & 0 \\ 1 & 0 & 0 & 0 \\ 0 & 0 & 0 & 1 \\ 0 & 0 & 1 & 0 \end{bmatrix}; \quad R_y = \frac{1}{\sqrt{8}}\begin{bmatrix} 0 & -i & 0 & 0 \\ i & 0 & 0 & 0 \\ 0 & 0 & 0 & -i \\ 0 & 0 & i & 0 \end{bmatrix}; \quad J_x = \frac{1}{\sqrt{8}}\begin{bmatrix} 0 & i & 0 & 0 \\ -i & 0 & 0 & 0 \\ 0 & 0 & 0 & -i \\ 0 & 0 & i & 0 \end{bmatrix}$$

$$J_y = \frac{1}{\sqrt{8}}\begin{bmatrix} 0 & 1 & 0 & 0 \\ 1 & 0 & 0 & 0 \\ 0 & 0 & 0 & -1 \\ 0 & 0 & -1 & 0 \end{bmatrix}; \quad M_x = \frac{1}{\sqrt{8}}\begin{bmatrix} 0 & 0 & 1 & 0 \\ 0 & 0 & 0 & 1 \\ 1 & 0 & 0 & 0 \\ 0 & 1 & 0 & 0 \end{bmatrix}; \quad M_y = \frac{1}{\sqrt{8}}\begin{bmatrix} 0 & 0 & -i & 0 \\ 0 & 0 & 0 & -i \\ i & 0 & 0 & 0 \\ 0 & i & 0 & 0 \end{bmatrix}$$

$$L_x = \frac{1}{\sqrt{8}}\begin{bmatrix} 0 & 0 & i & 0 \\ 0 & 0 & 0 & -i \\ -i & 0 & 0 & 0 \\ 0 & i & 0 & 0 \end{bmatrix}; \quad L_y = \frac{1}{\sqrt{8}}\begin{bmatrix} 0 & 0 & 1 & 0 \\ 0 & 0 & 0 & -1 \\ 1 & 0 & 0 & 0 \\ 0 & -1 & 0 & 0 \end{bmatrix}; \quad Q_z = \frac{1}{\sqrt{8}}\begin{bmatrix} 1 & 0 & 0 & 0 \\ 0 & -1 & 0 & 0 \\ 0 & 0 & -1 & 0 \\ 0 & 0 & 0 & 1 \end{bmatrix}$$

APPENDIX 3

The Commutation Relations $i[O, H]$ for the Operators O and the Hamiltonians $H = H_Q$, S_x, S_y, and S_z

	$i[O, H]$			
O	$H = H_Q$	$H = S_x$	$H = S_y$	$H = S_z$
C_x	0	$-\sqrt{3/2}\ L_x$	$-2C_z - \sqrt{3/2}L_y$	C_y
C_y	0	$2C_z - \sqrt{3/2}\ L_y$	$\sqrt{3/2}L_x$	$-C_x$
C_z	0	$-2C_y + \sqrt{3/2}R_y$	$2C_x - \sqrt{3/2}R_x$	0
T_x	0	$\sqrt{3/2}L_x$	$-\sqrt{3/2}L_y$	$3T_y$
T_y	0	$\sqrt{3/2}L_y$	$\sqrt{3/2}L_x$	$-3T_x$
T_z	0	$-\sqrt{3/2}R_y$	$\sqrt{3/2}R_x$	0
Q_z	0	$\sqrt{3}J_x$	$\sqrt{3}J_y$	0
R_x	$-2\sqrt{2}J_x$	L_x	$L_y - \sqrt{3/2}(T_z - C_z)$	R_y
R_y	$-2\sqrt{2}J_y$	$L_y - \sqrt{3/2}(C_z - T_z)$	$-L_x$	$-R_x$
J_x	$2\sqrt{2}\ R_x$	$M_x - \sqrt{3}Q_z$	$-M_y$	J_y
J_y	$2\sqrt{2}R_y$	$-M_y$	$M_x - \sqrt{3}Q_z$	$-J_x$
M_x	$-2\sqrt{2}L_x$	J_x	$-J_y$	$2M_y$
M_y	$-2\sqrt{2}L_y$	J_y	J_x	$-2M_x$
L_x	$2\sqrt{2}M_x$	$-R_x + \sqrt{3/2}(C_x - T_x)$	$R_y - \sqrt{3/2}(C_y + T_y)$	$2L_y$
L_y	$2\sqrt{2}M_y$	$-R_y + \sqrt{3/2}(C_y - T_y)$	$-R_x + \sqrt{3/2}(C_x + T_x)$	$-2L_x$

ACKNOWLEDGMENTS

Acknowledgment is made to the Donors of the Petroleum Research Fund, administered by the American Chemical Society, and the National Science Foundation National Young Investigator program (DMR-9458017) for support of this research. The solid state NMR spectrometer was purchased with a grant from the National Science Foundation (CHE-9405436).

REFERENCES

1. C. A. Fyfe, Y. Feng, H. Grondey, G. T. Kokotailo, and H. Gies, *Chem. Rev.* **91,** 1525 (1991).
2. W. Kolodziejski, P. J. Barrie, H. He, and J. Klinowski, *J. Chem. Soc. Chem. Commun.,* 961 (1991).
3. C. A. Fyfe, K. C. Wong-Moon, Y. Huang, and H. Grondey, *J. Am. Chem. Soc.* **117,** 10397 (1995).
4. H.-M. Kao and C. P. Grey, *J. Am. Chem. Soc.* **119,** 627 (1997).
5. G. A. Morris and R. Freeman, *J. Am. Chem. Soc.* **101,** 760 (1979).
6. (a) P. J. Chu, J. H. Lunsford, and D. J. Zalewski, *J. Magn. Reson.* **87,** 68 (1990). (b) P. J. Chu, A. de Mallmann, and J. H. Lunsford, *J. Phys. Chem.* **95,** 7362 (1991).
7. J. H. Lunsford, W. P. Rothwell, and W. Shen, *J. Am. Chem. Soc.* **107,** 1540 (1985).
8. A. J. Vega, *Solid State Nucl. Magn. Reson.* **1,** 17 (1992).
9. A. J. Vega, *J. Magn. Reson.* **96,** 50 (1992).
10. See, for e.g., C. P. Slichter, ''Principles of Magnetic Resonance,'' 3rd ed., Chap. 2, Springer, Berlin (1983).
11. N. Chandrakumar and S. Subramanian, ''Modern Techniques in High-Resolution FT-NMR,'' p. 357, Springer, Berlin (1987).
12. D. Fenzke, D. Freude, T. Frohlich, and J. Haase, *Chem. Phys. Lett.* **111,** 171 (1984).
13. (a) P. P. Man, *J. Magn. Reson.* **67,** 78 (1986). (b) P. P. Man, *Mol. Phys.* **76,** 1119 (1991).
14. (a) P. P. Man, *J. Magn. Reson. A* **114,** 59 (1995). (b) P. P. Man, E. Duprey, J. Fraissard, P. Tougne, and J.-P. d'Espinose, *Solid State Nucl. Magn. Reson.* **5,** 181 (1995).
15. H.-M. Kao and C. P. Grey, unpublished results.
16. P. J. Chu, R. R. Carvajal, and J. H. Lunsford, *Chem. Phys. Lett.* **175,** 407 (1990).